Available Online at www.ijcsmc.com

International Journal of Computer Science and Mobile Computing

A Monthly Journal of Computer Science and Information Technology

ISSN 2320–088X

IJCSMC, Vol. 3, Issue. 9, September 2014, pg.822 – 832

RESEARCH ARTICLE

Voice Based Guidance and Location Indications System for the Blind using GSM, GPS and Optical Device Indicator

Sama Santhosh Reddy[1], Mrs. G. Sathyaprabha[2], Mr. P.V. Vara Prasad Rao[3]

[1]M.Tech (ES&VLSI), SLC's Institute of Technology, JNTU, Hyderabad, India

[2]Assistant Professor (ECE), SLC's Institute of Technology, JNTU, Hyderabad, India

[3]Head of the Department (Digital Systems Computer Electronics), SLC's Institute of Technology, JNTU, Hyderabad, India

[1] sama.sanreddy@gmail.com

Abstract— An active optical pathfinder using a LED and a photodiode is implemented as an electronic travel aid to improve the mobility of persons who are blind. The protected path is optimized by using radiometric calculations. Protection zones for typical configurations of obstacles are studied: an opening, a side panel, a front panel, and a post. The results in real configurations such as parked cars, trees, and dustbins are presented too. Finally, we explain how the device can be used in real life by visually impaired people, in conjunction with the typical white stick.

Keywords— Blind people, electronic travel aid (ETA), infrared (IR) detection

I. INTRODUCTION

Walking safely and confidently without any human assistance in urban or unknown environments is a difficult task for blind people. Visually impaired people generally use either the typical white cane or the guide dog to travel independently [1]. Although the white stick gives a warning about 1 m before the obstacle, for a normal walking speed of 1.2 m/s, the time to react is very short (only 1 s). The stick scans the floor and consequently cannot detect certain obstacles (rears of trucks, low branches, etc.). Safety and confidence could be increased using devices that give a signal to find the direction of an obstacle-free path in unfamiliar or changing environments. Electronic travel aids (ETAs) are devices that give off a warning by auditory or/and tactile signals when an obstacle is in the way and allow the user to avoid it [1], [2].

Several devices have been developed to improve the mobility of blind people [3], [4]: talking GPS [5], devices for landmark identification (near-infrared (IR) light or radio frequencies) [6], [7], ultrasonic obstacle detectors (K sonar [8], Ultracane [9], Miniguide [10], Palmsonar [11], Ultra-Body-Guard [12], and iSonic cane [13]), and optical devices (the laser long cane [14]).
In indoor or outdoor crowded environments, ultrasonic devices are limited due to multiple reflections [4]. These devices cannot find openings that are wide enough for a human being to go through, with anticipation of a few meters (4–6 m). On the other hand, laser devices collect information about very narrow openings that are not large enough to be free paths. Therefore, they detect a lot of useless information (details of fences, of branches, of walls, etc.).

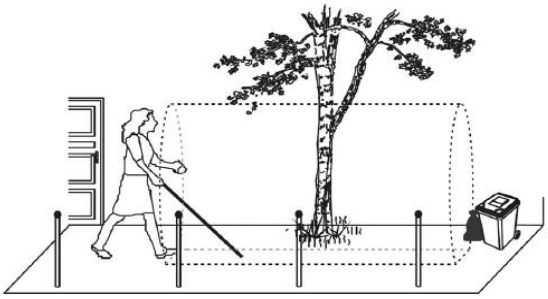

Fig. 1. Ideal protection volume (dashed lines).

Ideally, the detected path should be shoulder width, vertical from ground level to the level of the user's head, and up to a few meters ahead of the user, as shown in Fig 1. Our approach is to develop an active IR device to improve the rate of relevant detection in indoor and outdoor crowded environments. Our purpose is to detect shoulder-width openings that are a long distance away (4–6 m), without detecting openings that are too narrow (less than 0.5 m wide). The IR devices that we have been developing are the Tom Pouce and the Minitact. The aim of these devices is to protect users from obstacles that are at knee to head level. The device can be fastened to the cane or held by the user. It gives a vibrating warning when an obstacle is ahead of the white cane or of the hand. In outdoor situations, the Tom Pouce I (first generation) is fixed to the white cane at hand level. The cane and the device are continuously swept sideways. In this way, the unevenness of the ground is detected by the tip of the cane. High and horizontal obstacles are detected by the device. The permanent right and left scan of the device allows the user to perceive the direction of the various paths that are available, owing to a lack of vibrations.

According to user experiences, the largest range (4mfor Tom Pouce I) has been reported to be the most comfortable for stressfree walking. However, with this range, blind users generally claim that it is difficult to perceive narrow but still human-sized paths with 4-m anticipation. If the ETA does not detect a free path with such anticipation, the only way to go through is to assume that there is a path and to reduce the range of the ETA to keep looking for the freeway. For example, a 2-m range gives a shorter and narrower protection area. The benefits of the device are then highly reduced, because they may not be the free path. For the Tom Pouce I, it was not possible to give more than 4-m anticipation because the beam would detect the floor as being too wide.

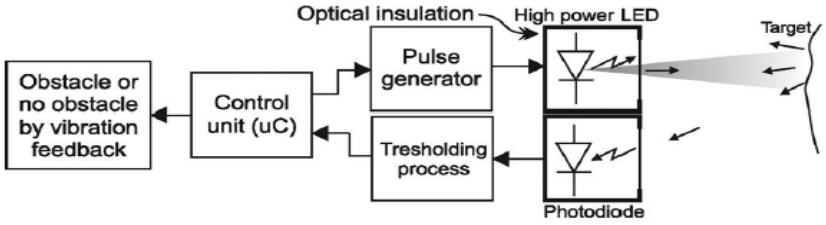

Fig. 2. Schematic diagram of the IR detector.

In the literature, ETAs are characterized by their detection ranges [2], [3], [8]–[14], but neither the width of the detection area nor the effective abilities and limits to detect paths are detailed. The divergence of the emitted beam is far from being satisfactory information to answer this question whatever technology is used. The purpose of this paper is to present a method to improve and approximate the "ideal" protection area, which is to have a narrower (such as shoulder width) and longer zone (Fig. 1). This method makes it possible to calibrate and control the dimensions of the protection area of the IR devices. Theoretical and experimental photometric results are presented and discussed. A practical device used by blind people in everyday life will finally be described, and current real-life obstacle configurations will be presented.

II. PRINCIPLE OF THE INFRARED DETECTOR

The device includes a near-IR LED and a photodiode (Fig. 2). The LED emits a train of pulses. These pulses strike the obstacle, and the retro diffused light is detected by the photodiode. The light detected is processed to determine whether there is a path or not.

The sensitive surface of the photodiode is placed next to the LED and perpendicularly to the axis of the LED beam. Both components are optically insulated and separated by 15 mm to prevent the emitted light from getting directly into the photodiode.

The LED emits pulses managed by a control unit. The control unit increases the amplitude of the pulse step by step. When the signal-to-noise ratio of the photodiode is high enough to detect the presence of the obstacle (detection threshold), the emission is interrupted. The last amplitude of emitted light gives a value. When this value is lower than a constant (arbitrarily fixed, which

we will call "range constant"), a vibration is sent to the user, which means that there is an obstacle. A lack of vibration means a free path, and the higher the constant, the larger the free path. The choice of the constant determines the range of the device (protection length). The constant and, therefore, the range will be adjustable by the user. In this system, the range depends on the albedos of the obstacles. In practice, this system gives efficient protection to blind people except in the case of specific obstacles, which we will describe in Section V-C.

III. RADIOMETRIC CONSIDERATION

To study how the protection area depends on the parameters of the LED and those of the obstacles, we calculate the irradiance on the detector to draw the theoretical protection area for planar obstacles.

Let $I(\theta)$ be the intensity distribution of a LED; the light that is retrodiffused by the target is detected by the photodiode of surface *dA*. The target is a planar surface that is in front of the sensor and is supposed to be a Lambertian surface of albedo ρ. Using a geometrical optics model [15], [16], the irradiance *E* on the detector is calculated.

The parameters of the setup are defined in Fig. 3. The LED is placed at origin *O* of the coordinates and emits a beam in direction (*Oz*), and the retrodiffused light is detected by a photodiode of area *dA* located close to the LED (15 mm). Let *P* be a plane situated at distance *D* from the sensor, *D* = *OH*, and θp be the angle between *OH* and the axis of the LED (*Oz*). *M* is the intersection point of the LED axis (*Oz*) with *P*, *l* = *OM*, *N*(*x*, *y*, *z*) is a current point on *P*, *da* is the elementary surface around N, $\vec{r} = \overrightarrow{ON}$, $\theta = (\widehat{ON}, \widehat{OM})$, $\hat{n}$ is the unitary vector perpendicular to *P* in *N*, and $\theta a = (\hat{}n, \_r)$. The equation of plane *P* is

$$z = l + x \tan \theta_p \qquad \forall y. \qquad (1)$$

According to the experimental setup, the LED and the photodiode are separated by 15 mm (on the *x*-axis). This distance is negligible compared with the distance of the obstacle (*l* _ 15 mm). Therefore, to facilitate calculation, we consider that the LED and the photodiode are located in the same place. The irradiance on *dA* of the light retrodiffused by the Lambertian plane *P* is given by

$$E = \frac{\rho}{\pi \cos \theta_p} \int_{x_0}^{x_1} \int_{y_0}^{y_1} \frac{I(\theta)}{z^4} \cos^2 \theta_a \cos^5 \theta dy dx \qquad (2)$$

where $z = l + x \tan \theta_p$

$$\cos \theta_a = \frac{x \sin \theta_p - (l + x \tan \theta_p) \cos \theta_p}{\sqrt{(l + x \tan \theta_p)^2 + x^2 + y^2}}$$

$$\cos \theta = \frac{l + x \tan \theta_p}{\sqrt{(l + x \tan \theta_p)^2 + x^2 + y^2}}.$$

The details of the calculus procedure are included in the Appendix.

IV. EXPERIMENTAL MEASUREMENTS AND SIMULATIONS

Equation (2) is the theoretical result for planar obstacles. For verification of these results, the shapes of the obstacles were taken into account, owing to the integration limits. A function of intensity distribution was established by the radiation pattern given by the LED manufacturer. This equation is neither a Lorentzian nor a Gaussian function: It is in between. A Pearson VII function was used because it showed the best fit to the LED emission curve. Moreover, a Pearson VII function can easily be modified by adapting its *m* parameter (3), from a Gaussian to a Lorentzian shape, and can fit all kinds of LEDs. The Pearson VII function [17], [18] is

$$I(\theta) = I_0 + A_c \frac{2\Gamma(m)\sqrt{2^{1/m} - 1}}{\sqrt{\pi} w \Gamma(m - 1/2)} \left[1 + 4\frac{2^{1/m} - 1}{w^2}\theta^2\right]^{-m}. \qquad (3)$$

*I*0 is the offset, *w* is the full-width at half-maximum of the curve, *Ac* is the amplitude, Γ is the Euler Gamma function $(\Gamma(m) = \int_0^\infty e^{-u} u^{m-1} du, m >; 0)$, and *m* is the shape parameter (*m* = 1 is a Lorentzian curve, and *m* = ∞ is a Gaussian curve). A diaphragm placed in front of the LED generates some apodization that limits the angular emission f the LED. An apodization function was introduced in (3). The apodization function is a rectangular function that sets the values of intensity to zero for angles greater than θL and does not change them for angles lower than θL.

The *m* values measured for the commercial LED currently vary between 0.7 and 300. The right *m* is chosen among the commercial available LEDs. The other adjustments are controlled by the electronics, standard optics, and apertures: Intensity *Ac* is controlled by the injection current in the LED, maximal angle emission θL of the LED is controlled by a diaphragm fixed to the output aperture of the device, and emission angle *w* at full-width at half-maximum intensity is controlled by the focal length of the optic associated to the LED.

The parameters of the source that were used for the theoretical calculations and experimental configurations were as follows: w = 0.10 rad, Ac = 0.74 W/sr, $I0$ = 0.02 W/sr, m = 1.39, and θL = 18◦ (changes on these values will be specified). The threshold of the detector (Eth) was set to 2.5 × 10−4 W/m2. LED pulses are interrupted once the detection threshold $E = E$th is reached. The LED pulses are driven by a control unit, and the forward voltage is variable; its maximum value is 3 V. The central wavelength of the LED is 950 nm, and the divergence of the emitted beam is 6◦. The current of the pulse varies according to the forward voltage between 20 mA and 1 A. To make a reproducible setup to draw the protection zone, two 1 m × 2 m panels covered with a white mat paper were constructed. This paper is a Lambertian surface of 0.99 albedo. Basic configurations were reproduced: a lateral obstacle and a frontal obstacle, an opening, and an oblique plane.

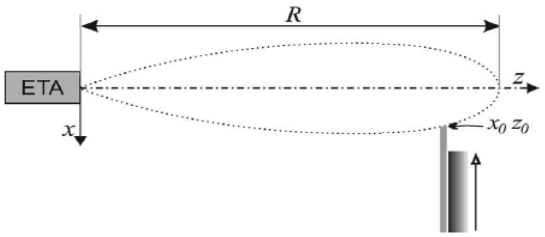

Fig. 4. Experimental setup for the study of the side panel.

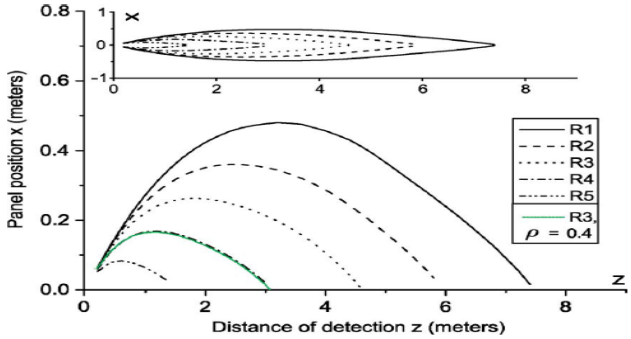

Fig. 5. Theoretical protection curves for the side panel; in the upper part of the graphic, the curves are drawn with a proportional x, z scale. For $R1$–$R5$ curves ($\rho = 1$), another curve $R3$ with $\rho = 0.4$ albedo is confounded with $R4$.

A. Case of a Lateral Panel

The ETA was placed 1 m above the ground. A 1 m × 2 m panel was moved perpendicularly to the optical axis (Oz) of the beam. The position of the edge of the panel was noted ($x0$, $z0$) when the device started to vibrate (Fig. 4). The limits of integration for the theoretical case (2) were as follows: [$x0$, $x0$ + 1 m] for x and [−1 m, 1 m] for y, $z0$ was fixed, and $x0$ was given by (2) for $E = E$th. The procedure was repeated for five theoretical values of the "range constant" (defined in Section II) corresponding to ranges $R1$, $R2$, $R3$, $R4$, and $R5$, respectively. The results are shown in Fig. 5.

The theoretical and experimental results are shown in Fig. 6 for the following values: w = 0.1 rad, $I0$ = 0.02 W/sr, θL = 18◦, and Ac corresponding to ranges $R5$ and $R3$ with$m$ = 1.39 and 4.5, respectively

B. Case of an Opening

Two panels were placed simulating an open door. The separation between them was set to d (Fig. 7). The ETA was placed 12 m from the panels, and distance $z2$ was found by bringing the device close to the opening, following axis z until there was some vibration; then, $z2$ was noted. The distance to the panel z was further reduced, and $z1$ was noted when the vibration stopped. Therefore, in order to draw the entire protection area, the distance d was changed, and the entire process was repeated.

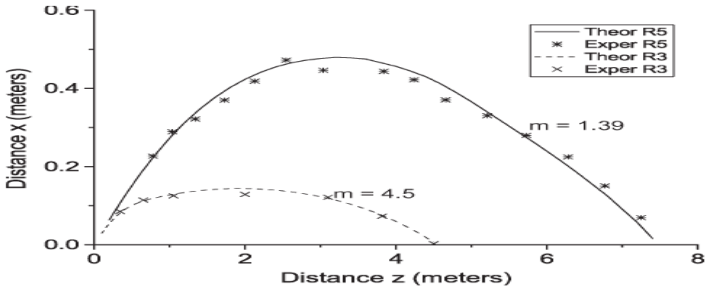

Fig. 6. Theoretical and experimental results for the lateral panel.

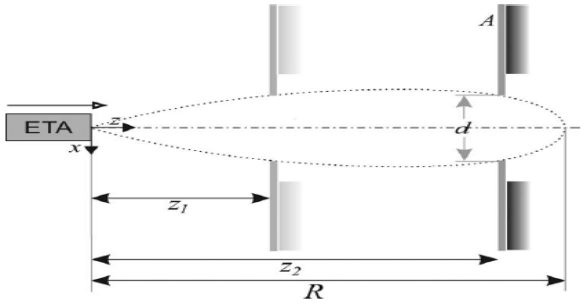

Fig. 7. Setup of a protection zone in the case of an open door.

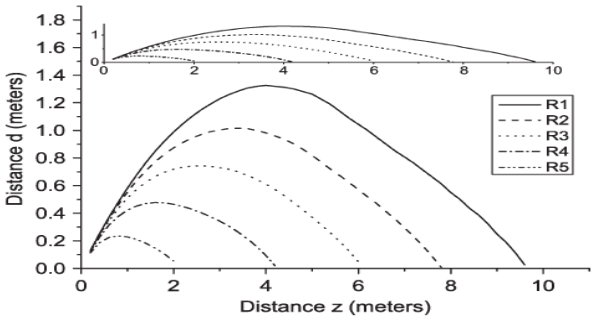

Fig. 8. Theoretical protection curves of the openings for five ranges; in the upper part of the graphic, the curves are drawn with a proportional x, z scale.

The theoretical case was calculated by integrating (2) in two parts: the left side and the right side of the panel. The calculations were made for five values of emission power, and their experimental correspondences were measured. The theoretical results are shown in Fig. 8. Fig. 9 shows the theoretical and experimental results for w = 0.1 rad, $I0$ = 0.02 W/sr, θL = 18◦, and the value of Ac corresponding to $R3$ with m = 1.39 and m = 4.5.

C. Albedo and Panel Size Dependence

The ability of the device to detect a panel ahead of the user depends on the size, the reflectivity, the incidence angle, and the emission power of the LED. Equation (2) was used to calculate the detection distance (using $R1$) of a 2-m-high panel as a function of its width and albedo (Fig. 10). Thus, a 1-m-wide panel with a 0.99 albedo was detected 8 m away, but it would be detected 3 m away if its albedo was 0.1. According to Fig. 10, when the width of the panel is known, the detection distance can be predicted. The detection distance as a function of the color of a panel has been measured. A 1 m × 1 m panel made of 160 g/m2 colored paper was used. The results are shown in Fig. 11.

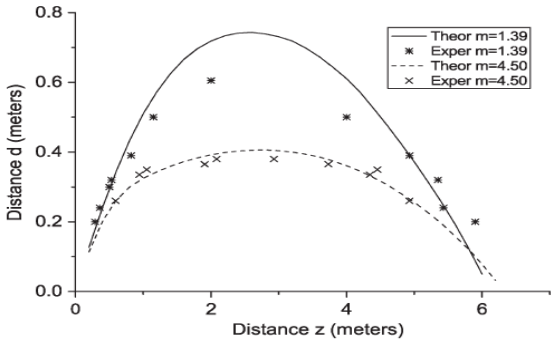

Fig. 9. Experimental and theoretical results for the opening (range $R3$).

D. Oblique Panel

Fig. 12 shows that the detection distance of the panel varies according to the incidence angle θp of the panel (Fig. 4) with the axis of the device and with the range.

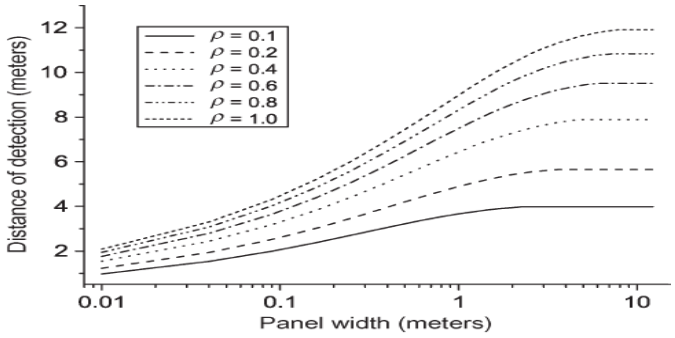

Fig. 10. Detection of a 2-m-high frontal panel of varying width.

E. Real Obstacles

To highlight the protection zone for real obstacles, typical everyday-life situations were analyzed for indoor conditions, i.e., a narrow path and an open door, and for outdoor conditions, i.e., a sidewall with and without garbage and cars from different side views. The measurement process was the following: The user had been walking in a given direction sweeping the device, and at the very moment that he noticed a change in the directions indicated by the device giving vibrations, he stopped and the directions with and without vibrations were measured.

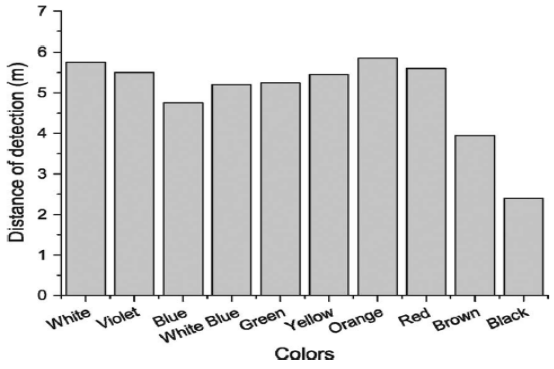

Fig. 11. Detection distance of a 1 m × 0.65 m panel for different colors (6-m range).

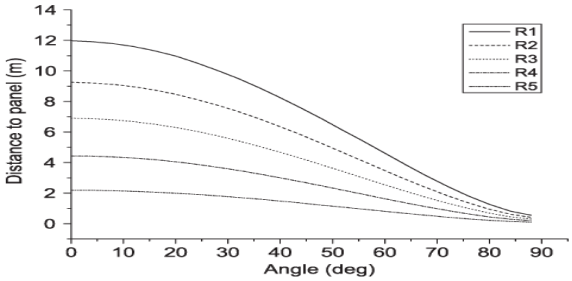

Fig. 12. Detection of a panel at varying incidence angles for $\rho = 1$ for each range.

F. Indoor Situation

These situations involved a person walking along a corridor with a 4-m range (*R*4). In Fig. 13(a), we suppose that the path without vibration is wide enough to consider a lateral tilted wall on one side and a lateral panel on the other side. If the path had been narrower, we would have chosen the model of an opening. For the lateral wall on the right side, the direction of the beginning of the vibration makes a 76◦ angle with the wall. For a 4-m range, the curve in Fig. 13(a) indicates a 75-cm distance to the wall for a white wall (*albedo* = 1), a value that agrees with the experiment. Regarding the 50◦ tilted cardboard box pile (albedo measured is 0.92 at 950 nm) on the left, we consider it as a side panel of albedo of 0.92 cos2(50◦) = 0.4, taking the tilt into consideration. The half-width of the beam is 1.5 cm, which is in agreement with a vibration limit very

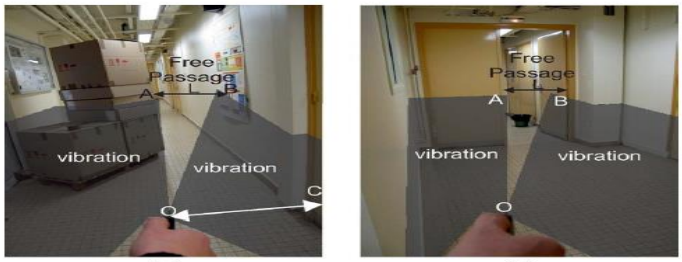

Fig. 13. Typical obstacles in a corridor; the range of the device is 4 m. (a) Narrow path in a corridor: $A = 3$ m, $B = 3$ m, $L = 0.6$ m, and $C = 0.75$ m (distance to the right wall). (b) Lateral open door in a corridor: $A = 3.6$ m, $B = 3.7$ m, and $L = 0.8$ m.

Fig. 14. Sidewalk with and without garbage bin. (a) $A = 5$ m, $B = 0.85$ m, and $\alpha = 80°$. (b) $A = 3.25$ m, $B = 0.85$ m, $C = 0.75$ m, and $\alpha = 88°$.

close to the direction of the far end of the pile (4 cm). Similar considerations can be made for Fig. 13(b).

G. Outdoor Situation

The most common outdoor situation is walking on a sidewalk, where cars and garbage bins are found. First, situations of a wall with and without a garbage bin were analysed [Fig. 14(a)]; then, those of a car from two side views were analyzed.
The presence of a garbage bin gives an 8◦ difference in the angular perception of the lateral wall. In practice, this is sufficient to be clearly perceived by users [Fig. 14(b)]. For cars in the front view [Fig. 15(a)], the color of the car is not very important, as long as the hood of the car is a tilted plane; the main contribution to the signal is the number plate, which is a standard object. At the very moment that the car is detected, the direction indicated by a lack of vibration gives a straight-line obstacle-free path. For a car from a side view [Fig. 15(b)], the first path indicated is still in the direction of the wing of the car. Therefore, the user will deviate and deviate again when he is closer to the car. The avoidance trajectory drawn by the user will be a curve whose curvature is in the direction of the car.

V. DISCUSSION

The adjustment of the shape of the protection area, the limits of the device, the real situations, and the consequences for the mobility of blind people are discussed.

Fig. 15. Car detection. (a) Front view: $d = 6.5$ and $A = B = 0.2$ m. (b) Side view: $A = B = 5.2$ m, $C = 1.3$ m, and $d = 5$ m.

A. Parameter Dependence

The main parameters that determine the shape of the protection zone of the device are the intensity distribution of the source (3): full-width of the beam at half-maximum *w*, amplitude of emission *Ac*, shape parameter *m*, and apodization angle (given by the mechanical aperture ahead the LED limiting the angular width of the beam).

The variation of these parameters allows the detection zone to be controlled. Parameter *w* permits the width of the protection zone to be controlled, without much influence on the length [Fig. 16(a)]. Amplitude *Ac* increases length and width at the same time [Fig. 16(b)]. The apodization angle controls the width of the protection zone at short distances and does not change its length [Fig. 16(c)], and the shape parameter *m* modifies the width of the protection zone [Fig. 16(d)]. The five theoretical ranges shown in Figs. 6 and 9 are representations of the relative distances for finding the obstacles with different amplitudes *Ac* of emission.

B. Influence of External Parameters

The shape of the protection zone is modified by external parameters; the light that strikes the surface can be absorbed, transmitted, and reflected. The surface analyzed is considered as a Lambertian plane in our statements, but in real configurations, some parts of many objects are reflective, and others are diffusive, retroreflective, etc. The light spot on the target has a given width, generally greater than the details of the obstacles. Therefore, it can be represented by an average albedo. Sunlight is another external parameter that introduces additional noises as it contains the same wavelength as the LED. The sensitivity of the photodiode is then decreased on sunny days. To solve this problem, a phototransistor has been incorporated to measure the diurnal light. The amplitude of the emitted pulse of the LED and the threshold have to be increased to keep the same signal-to-noise ratio. A calibration table has been saved in the control unit memory. The table is read according to the signal of the phototransistor to keep the same characteristics of detection whatever the ambient light may be.

C. Low Albedos and Retroreflective Surfaces

Fig. 10 shows the variation of the range according to the albedo. The consequence of a reduction by ten of the albedo is a reduction of three in the distance of anticipation. In current situations, the color of the obstacle does not have a lot of influence on the detection distance except for very dark obstacles (Fig. 11). A small change in the anticipation distance does not affect walking fluidity. However, a thin shiny black vertical rod is a specific case, and anticipation can be too short. The white cane may come into contact with the post before warning is given off by the detector.

Another specific case is retroreflective surfaces such as vehicle number plates and road signs. Such panels can be detected with 20-m anticipation, whereas a Lambertian surface would be detected 7 m away. In practice, these surfaces make it possible to detect and anticipate vehicles from a long distance. Table I shows real anticipation distances with a range of 6 m.

D. Real Situations

In spite of the simple situations used for the theoretical model, it allows typical real situations to be interpreted. The most important situation when the device is not efficient is sidewalks with thin dark posts. The problem can be solved owing to an additional triangulating laser telemeter, without losing the benefit of the IR sensor, i.e., finding a shoulder width path from a distance exceeding 4 m without perceiving the small details that do not help walking.

E. Mobility Aspects

Blind people detect obstacles by sweeping their white sticks and by making contact with obstacles. In the worst case scenario, they get hurt, particularly by objects which are located in a high position, such as rears of trucks, branches, advertising boards, etc. These obstacles are a source of stress for blind people when they are walking. The IR device is attached to the white stick with its emission axis placed horizontally. As the user sweeps the white stick to detect obstacles, the system scans in every direction that is taken by the stick; hence, the horizontal protection zone is enlarged (Fig. 17). Making a sweep of $\pm 10^{\circ}$ (with the standard length of the cane fitted to the height of he user, $\pm 10^{\circ}$ corresponds to the width of the feet), the tip of the stick protects the user from the hazard of holes. Thus, the user's body is protected by the IR detector, which anticipates the obstacles.

The horizontal detector placed on the cane at about 1 m high does not give a protection area large enough to protect the head (Fig. 9). To solve this problem, we have added a second range *R*3 detector, tilted vertically by 30◦ to protect the head. Using the

device requires a training process. The technique to anticipate a side panel, i.e., sweeping the white stick, is quite different from the technique to detect an opening. For a side panel, the device gives off a vibration on one side of the path, and the user must change directions until the vibration remains turned off during the whole sweep of the stick. To find an opening, the user has to perceive a lack of vibration between two side vibrations. When the blind user is walking along a path where there are no vibrations, in ranges *R*1–*R*4 (down to 4 m), his/her shoulders are protected even if the perceived path is very narrow (Fig. 8).

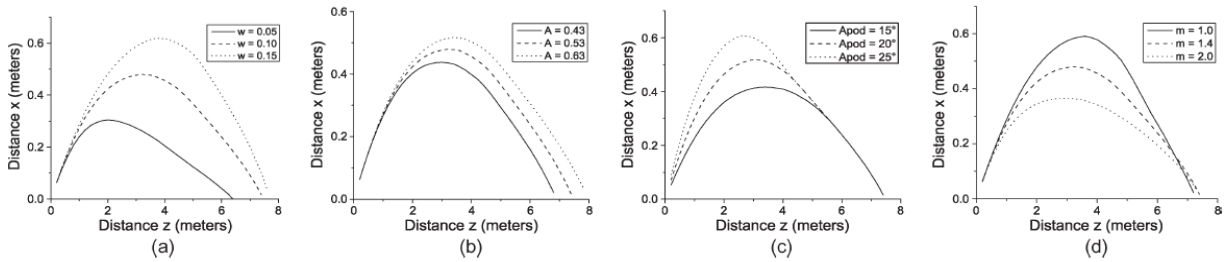

Fig. 16. Variations of the protection area as functions of its parameters. (a) Width of emission. (b) Amplitude A_c. (c) Apodization angle θ_L. (d) Shape parameter m.

TABLE I
SOME TYPICAL OBSTACLES IN A STREET

Obstacles	Anticipation (m)	Description
Aluminium post	2.0	Diameter: 13cm
Dark shiny post	1.5	Diameter: 13cm
Dark shiny post	0.8	Diameter: 8cm
Wooden post	2.5	Diameter: 20cm
Big dustbin	3.2	0.45m×1m×1.5m
Tree trunk	3.9	Diameter: 30cm
Tree trunk	4.2	Diameter: 60cm
Vehicle front side	7.0	
Vehicle back side	14.0	
Vehicle lateral side	3.0	

The relative ranges used in the current device Tom Pouce II and Minitact are, finally, 6, 4, and 2 m. These ranges are chosen by the user according to his/her speed and the density of obstacles along the path.

We have tested two commercially available ultrasonic devices: the Palmsonar and the Miniguide. The test was performed to detect an open door with a width of 0.83 m. The measurement showed us that the Miniguide and the Palmsonar do not detect the difference between an open door and a wall for ranges longer than 0.9 and 1.8 m, respectively. However, the Minitact can detect an opened door with a 6-m range.

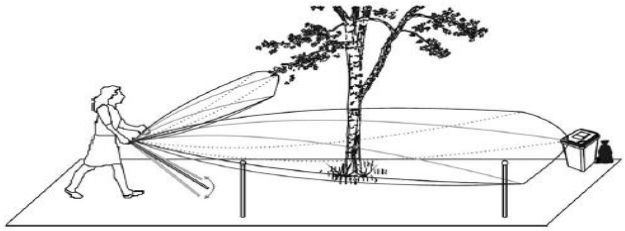

Fig. 17. Protection area generated by the sideways movement of the long cane.

Fig. 18. Actual devices: Minitact and Tom Pouce II. (a) Minitact used without cane for indoor use. (b) Tom Pouce II is fixed to the cane, and the vibration is external to avoid the confusion with the vibration of the cane in contact with the floor. A switch under the thumb is used to change the range.

CONCLUSION

Typical obstacles (walls, openings, and vertical rods) have been used to draw the protection zone of the IR device. The ability of the IR sensor to find a path wide enough for a person to go through has been demonstrated. Theoretical and radiometric calculations based on optical geometry have been made to improve the design and performance of the system.

The importance of intensity distribution to determine the protection zone has been highlighted. The technical compromises used in our new generation of IR devices have been presented. The data of the LED given in Section IV are those of the final parameters for the devices. The newest versions of the Tom Pouce II [Fig. 18(b)] and Minitact [Fig. 18(a)] devices [19] have been improved owing to the calculations presented in this paper; the Minitact only has a horizontal beam, it is smaller than the Tom Pouce II, and it is generally used inside. The Tom Pouce II has a second beam for the height, it is fixed to the cane, and it is used more outside (Fig. 17). These devices will progressively replace the Tom Pouce I, including a population of around 600 visually impaired people.

Very thin obstacles such as shiny dark posts are difficult to detect with enough anticipation (only 1.5 m). To solve this problem, a triangulation laser telemeter can be added. The triangulation laser telemeter can detect a shiny dark post up to 8 m away, and it is a good complement to the IR device. Since 1998, we have developed laser telemeters that are attached to the white stick, and the devices have helped blind people to anticipate obstacles [20]–[22].

In the near future, we are going to propose a device including the laser telemeter and various IR detectors: The laser detects small parts with low albedos, and the IR detector finds obstacle-free paths that are wide enough for a person to go through.

APPENDIX A
PROOF OF THE IRRADIANCE EQUATION TO DETECT A PLANE SURFACE

In Fig. 2, da is the differential area on the tilted plane, so the power received by da is

$$d\phi_{da} = I(\theta)d\Omega \tag{A1}$$

with $d\Omega = da\cos\theta_a/r^2$ and $r = z/\cos\theta$.

The irradiance on da is therefore E_{da}

$$E_{da} = \frac{d\phi_{da}}{da} = \frac{I(\theta)}{z^2}\cos\theta_a\cos^2\theta.$$

The plane is considered to be a Lambertian surface. Therefore, its radiance is $L_{da} = \rho E_{da}/\pi$

$$L_{da} = \frac{\rho I(\theta)}{\pi z^2}\cos\theta_a\cos^2\theta.$$

Let $d\phi_{da}$ be the power arriving on dA from da

$$d\phi_{da} = L_{da}\frac{da\cos\theta_a dA\cos\theta}{r^2}$$

where

$$d\phi_{da} = \frac{L_{da}}{z^2}\cos\theta_a\cos^3\theta dadA$$

replacing L_a in $d\phi_{da}$

$$d\phi_{dA} = \frac{\rho I(\theta)}{\pi z^4}\cos^2\theta_a\cos^5\theta dadA.$$

The irradiance on dA is

$$E = \frac{\rho}{\pi\cos\theta_p}\int_{x_0}^{x_1}\int_{y_0}^{y_1}\frac{I(\theta)}{z^4}\cos^2\theta_a\cos^5\theta dydx \tag{A2}$$

where $\cos\theta_a = \hat{n}\cdot\vec{r}/r$, with $\hat{n} = \sin\theta_p\hat{x} - \cos\theta_p\hat{z}$; therefore

$$\cos\theta_a = \frac{x\sin\theta_p - (l + x\tan\theta_p)\cos\theta_p}{\sqrt{(l + x\tan\theta_p)^2 + x^2 + y^2}}.$$

Angle θ is

$$\cos\theta = \frac{l + x\tan\theta_p}{\sqrt{(l + x\tan\theta_p)^2 + x^2 + y^2}}.$$

REFERENCES

[1] B. Blash, W. Wiener, and R. Welsh, Foundations of Orientation and Mobility, 2nd ed. New York: AFB Press, 1997.
[2] U. Roentgen, G. Gelderblom, M. Soede, and L. de Witte, "The impact of electronic mobility devices for persons who are visually impaired: A systematic review of effects and effectiveness," J. Vis. Impairment Blindness, vol. 103, no. 11, pp. 743–753, 2009.
[3] U. Roentgen, G. Gelderblom, M. Soede, and L. de Witte, "Inventory of electronic mobility aids for persons with visual impairments: A literature review," J. Vis. Impairment Blindness, vol. 102, no. 11, pp. 702–724, 2008.
[4] N. A. Giudice and G. E. Legge, .
[5] R. Kowalik and S. Kwasniewski, "Navigator—A talking GPS receiver for the blind," in Computers Helping People with Special Needs, K. Miesenberger, J. Klaus, W. Zagler, and D. Burger, Eds. Heidelberg, Germany: Springer Berlin, 2004, ser. Lecture Notes in Computer Science, p. 626.
[6] M. E. Peck, "RFID tags guide the blind," IEEE Spectrum, New York, Tech. Rep., Jan. 2008.
[7] M. Saaid, I. Ismail, and M. Noor, "Radio frequency identification walking stick (RFIWS): A device for the blind," in Proc. 5th Int. CSPA, Mar. 2009, pp. 250–253.
[8] Bay advanced technologies The Bat K-Sonar. [Online]. Available: http://www.batforblind.co.nz/
[9] Gismag Ultracane Uses Ultrasonic Echoes to Offer Spatial Awareness to the Vision-Impaired. [Online]. Available: http://www.gizmag.com/ go/3827/
[10] G. R. Co. The Miniguide Ultrasonic Mobility Aid. [Online]. Available: http://www.gdp-research.com.au/minig_1.htm
[11] Takes Corporation, Owner's Manual: Palmsonar ps231-72009. [Online]. Available: http://www.palmsonar.com/231-7/prod.htm
[12] RTB The Ultra Body Guard. [Online]. Available: http://www.rtb-bl.de/ RTB/ultra-body-guard-2/?lang=en
[13] PRIMPO ISONIC: State of the Art Electronic White Cane. [Online]. Available: http://www.primpo.com/eng/products/isonic.html
[14] VISTAC. [Online]. Available: http://www.vistac.de/
[15] W. L. Wolfe, Introduction to Radiometry. Bellingham, WA: SPIE Publ., 1998.
[16] J. L. Meyzonnette and T. Lépine, Bases de Radiomètrie Optique, 2nd ed. Toulouse, France: Cépaduès, 2001.
[17] K. Pearson, "Mathematical contributions to the theory of evolution, xix: Second supplement to a memoir on skew variation," Philos. Trans. Roy. Soc. Lond. (A), no. 216, pp. 429–457, 1916.
[18] I. Takashi, "New measures of sharpness for symmetric powder diffraction peak profiles," J. Appl. Crystallogr., vol. 41, no. 2, pp. 393–401, 2008.
[19] H. H. et aides techniques Alarme D'Obstacle Tom Pouce Light. [Online]. Available: http://www.handicat.com/at-num-20714.html
[20] R. Farcy, B. Denise, and R. Damaschini, "Triangulating laser profilometer as navigational aid for the blind: Optical aspects," App. Opt., vol. 35, no. 7, pp. 1161–1166, Mar. 1996.
[21] R. Farcy and R. Damaschini, "Triangulating laser profilometer as a threedimensional space perception system for the blind," Appl. Opt., vol. 36, no. 31, pp. 8227–8232, Nov. 1997.
[22] L. A. C. C. Instrumental. [Online]. Available: http://www.lac.upsud. fr/teletact/index-teletact.htm

